Molecules can be sputtered also from pure metals: Sputtering of beryllium hydride by fusion plasma–wall interactions

Article *in* Plasma Physics and Controlled Fusion · June 2013

DOI: 10.1088/0741-3335/55/7/074004

CITATIONS
13

READS
98

7 authors, including:

D. Borodin
Forschungszentrum Jülich
111 PUBLICATIONS **832** CITATIONS
SEE PROFILE

R.K. Janev
Macedonian Academy of Sciences and Arts
392 PUBLICATIONS **5,632** CITATIONS
SEE PROFILE

Kai Nordlund
University of Helsinki
629 PUBLICATIONS **15,014** CITATIONS
SEE PROFILE

Molecules can be sputtered also from pure metals: sputtering of beryllium hydride by fusion plasma–wall interactions

2013 Plasma Phys. Control. Fusion 55 074004

(http://iopscience.iop.org/0741-3335/55/7/074004)

Plasma Phys. Control. Fusion **55** (2013) 074004 (8pp) doi:10.1088/0741-3335/55/7/074004

Molecules can be sputtered also from pure metals: sputtering of beryllium hydride by fusion plasma–wall interactions

C Björkas[1,2], D Borodin[2], A Kirschner[2], R K Janev[2,3], D Nishijima[4], R Doerner[4] and K Nordlund[1]

[1] Association EURATOM-Tekes, Department of Physics, University of Helsinki, POB 64, Helsinki 00014, Finland
[2] Institute of Energy and Climate Research-Plasma Physics, Forschungszentrum Jülich GmbH, Association EURATOM-FZJ, Partner in the Trilateral Euregio Cluster, Jülich, Germany
[3] Macedonian Academy of Sciences and Arts, POB 428, 1000 Skopje, Macedonia
[4] Center for Energy Research, University of California at San Diego, La Jolla, CA 92093, USA

E-mail: carolina.bjorkas@helsinki.fi

Received 29 September 2012, in final form 5 November 2012
Published 14 June 2013
Online at stacks.iop.org/PPCF/55/074004

Abstract
The low-energy erosion mechanisms of first-wall materials subject to a fusion plasma are poorly known theoretically, even though they pose a critical problem for the development of tokamak-like fusion reactors. Using molecular dynamics computer simulations and analytical theory, we have examined the fundamental mechanisms of the erosion of first-wall materials, focusing on molecular release from beryllium surfaces. We show that the observed sputtering of BeD molecules from beryllium when exposed to a D plasma can be explained by the swift chemical sputtering mechanism, and that it also can happen in BeW alloys. This demonstrates that pure metals can, in contrast to conventional wisdom, be sputtered chemically. We also link the simulations of BeD sputtering to the plasma impurity transport code ERO, in order to follow the behavior of sputtered BeD species in a plasma. This multi-scale approach enables direct comparisons with experimental observations of BeD sputtering in the PISCES-B facility.

(Some figures may appear in colour only in the online journal)

1. Introduction

The success of future fusion devices such as ITER relies on a complete control of the plasma and its inevitable interactions with the vessel walls. This control requires a thorough understanding of the basic mechanisms occurring during plasma–wall interactions (PWIs). Erosion of the wall materials is one of the most crucial PWI events, which can seriously reduce the life time of components, degrade the plasma performance and enhance the long-term tritium inventory via co-deposition with eroded material [1, 2]. With increasingly advanced experimental techniques and theoretical expertise, more and more processes affecting the erosion are identified, taking us farther away from a simple and universal picture. Such processes are for instance enhanced re-erosion of re-deposited material [3], sub-surface bubbles [4], material mixing and alloying [5–7], fuzz formation [8] and molecular or chemical sputtering [9–11].

Molecular sputtering was observed in carbon materials long ago [9, 11–13]. The release of methane and hydrocarbon radicals even at very low incident ion energies is one of the main drawbacks of carbon, as it assists in the storing of radioactive tritium in the vessel walls. Recently, also Be has been observed to sputter molecules when subject to a D plasma [14–16]. On the other hand, mixing effects are relevant as different materials are foreseen for different reactor areas, and due to erosion and subsequent deposition, layers containing mixtures of the various components will form. In the case of ITER, these layers could be BeW alloys (Be_2W, $Be_{12}W$) [17–19], hydrogenated amorphous carbon layers or BeC mixtures [20] coming from the Be first wall and the C–W containing divertor. The erosion behavior from mixed

materials can be very different from that of the pure elements, as preferential sputtering of the lighter material can occur [21], rendering the process truly dynamic, and also making under some circumstances the suppression of chemical sputtering of carbon possible [22].

This work aims at improving the understanding of molecular sputtering from Be-based materials. The basic sputtering mechanisms at low-energy impact are reviewed and a simple model is applied to illustrate the sputtering mechanism present not only in both C and Be but also in BeW alloys. Molecular dynamics (MD) simulations are applied to D bombardment of Be and Be_2W and the BeD sputtering is quantified. Furthermore, ERO simulations are performed with the help of MD results to reproduce observations of BeD release in PISCES-B.

2. Bond breaking sputtering mechanism

The release mechanisms of substrate atoms due to ion bombardment are many and not always easy to identify and quantify. Which mechanism causes a specific sputtering depends on various variables, such as incoming particle energy, surface temperature, atomic configuration and structure of the substrate material. Even if restricting oneself to the fusion PWI regime, i.e. where the impact energy is low (<100 eV), the situation is complicated.

The perhaps simplest method of releasing atoms from a surface is through collisions. If enough energy (above the surface binding energy) is transferred either directly from the impinging ion to a surface substrate atom, or via subsequent collisions within the substrate, an atom can be sputtered. This mechanism is called *physical sputtering* and due to its nature it can be modeled using binary collision approximation codes such as SDTrimSP [23].

More intricate mechanisms are responsible for the release of non-volatile molecules from various surfaces. For instance, MD simulations have shown that dimers can sputter via the *dimer sputtering mechanism* in Cu [24] and WC [25]. The application of MD also has led to the identification of the mechanism behind hydrocarbon release from carbon surfaces at ion energies far below the physical threshold energy and at low substrate temperatures [26–28]. This mechanism was aptly named *swift chemical sputtering (SCS)* and is not to be confused with chemical erosion which includes thermally released volatile species.

The surface morphology of a material is intricate, but to understand the origin of the SCS, one can consider a simplified situation where a D ion is trying to break a single dimer bond (e.g. carbon dimer) by moving directly toward the center of the bond. The momentum transfer from the D ion to the dimer in the lateral direction can be expressed as

$$p_y = \int_{-\infty}^{\infty} f_y(t, E_{\mathrm{kin}}^{\mathrm{D}})\,\mathrm{d}t \approx \bar{f}_y \bar{\tau},$$

where f_y is the force acting on the dimer atoms and $E_{\mathrm{kin}}^{\mathrm{D}}$ is the initial kinetic energy of the D ion. $\bar{f}_y$ is an effective average force during the collision and $\bar{\tau}$ is the time which the D ion spends between the dimer atoms [28]. Three regions of interest

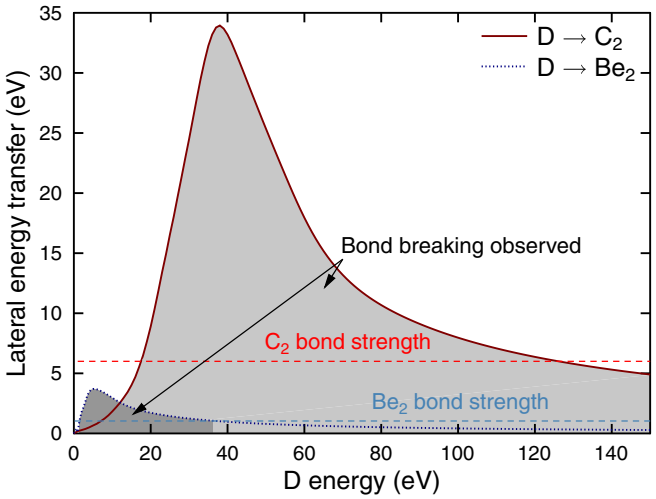

Figure 1. Lateral energy transfer to a C_2 and Be_2 dimer. The shaded areas indicate the interval at which bond breaking was observed. Data from [26].

can be extracted. (1) The incoming energy of the D ion is so low that it is reflected backward without entering the area between the dimer atoms. The dimer stays intact. (2) The ion energy is high enough to enter the bond area and the dimer bond breaks. (3) The energy is so high that the D ion quickly passes through the bond area and $\bar{\tau}$ is therefore too short (on the order of below 10 fs) for causing the bond to break. As such, there is a finite ion-substrate-dependent energy window for bond breaking to occur.

Figure 1 illustrates the energetics characteristic of the bond breaking of a C_2 and Be_2 dimer. The data plotted in the figure are obtained by impinging a D ion directly at the center of the dimers and observing the outcome [26]: the fate of the D ions is reflection, penetration or sticking and the dimer either stays bonded or breaks up. These simulations were carried out with the MD code PARCAS [29] using classical interatomic potentials [30, 31]. The figure shows the lateral energy transfer, which is calculated by subtracting the final energy for motion in the direction perpendicular to the motion of the incoming D from the total energy of each dimer. The gray areas indicate the energy interval at which bond breaking was observed and the dashed lines mark the bond strengths of the two dimers. The plot highlights the fact that the crucial parameter in the bond breaking mechanism is the momentum transfer from the ion to the dimer, since the agreement between the gray area and the position at which the bond energy line crosses the lateral energy transfer curve is excellent. Supporting this is also the fact that the energy window is limited, meaning that at very high energies, the momentum transfer becomes very low for bond breaking to happen as explained above. The same plot for the BeW dimer (not shown here) shows that bond breaking occurs in the energy range ∼11–34 eV and that below 17 eV, the D ion also becomes attached to either Be or W [26].

Since SCS involves bond breaking, it was initially believed that it is natural only to covalent materials such as carbon and silicon and that it would not occur in metals due to their non-directional bonding [32]. According to the simple model

above, the only difference between breaking a C and Be dimer bond is the required energy (the C dimer is much more strongly bonded), and therefore SCS could also take place in Be, or in mixed BeW and BeC alloys. (A bond in metals is here defined as the attraction between lattice atoms.) Bond breaking for a pure W material, on the other hand, is according to the same model highly unlikely due to large mass differences and related weak momentum transfer. In the next section, we show that it is indeed possible for low energetic 7–200 eV D to release molecules from Be and BeW surfaces through the SCS and that this mechanism can explain the observed release of BeD molecules from Be surfaces [15, 33].

3. MD simulations of D bombardment of Be and BeW surfaces

A surface of a wall material is very different from a collection of dimers, therefore the simple model described above does not reveal the whole story of how, e.g., C or Be is sputtered due to D ion impact. For instance, the coordination number Z of atoms located at the surface changes during bombardment (in the Be case, it could range from only 1 to the ideal surface coordination $Z = 9$ or bulk hcp $Z = 12$), atoms can be manifold connected to not only other substrate atoms but also to added plasma or impurity atoms, hydrocarbon chains are common on hydrogenated carbon surfaces, sub-surface bubbles can form and the surface can be depleted on substrate atoms if the incoming ion flux is very high. All of this affects the ability of the substrate atom to be sputtered. Therefore, to imitate a more realistic PWI situation, cumulative bombardments of low-energy (7–200 eV) D ions impacting on a Be and Be_2W surface were simulated using MD.

3.1. Simulation setup

A slab of dimensions $x = 25$, $y = 28$, $z = 40$ Å represented a tiny part of a Be wall in the simulations. This cell consisted initially of 3388 Be atoms organized in an hcp lattice with an open (0 0 0 1) surface. The Be_2W simulation cell on the other hand consisted of a Be_2W lattice (one of the few stable BeW alloys [34]) with 3079 atoms arranged in the $MgZn_2$/C14 crystallic configuration with dimensions $x = 28$, $y = 32$, $z = 39$ Å. Surfaces terminated with both a W or Be upmost layer were bombarded.

Plasma impact was modeled by cumulative D bombardments with impact energy in the range 7–200 eV. The cumulative nature of the simulations combined with extensive computational cost per impact imposed restrictions on the flux and fluence of the incoming ions: 3000 bombardments were performed with a flux of $\sim 2 \times 10^{28}$ m^{-2} s^{-1}. A uniform bombardment was simulated by shifting the cell randomly in x and y directions before each impact. The whole cell was also allowed to relax at 300 K (or alternatively 450, 725 K) for 2 ps in between. One bombardment lasted 7 ps in total. Fixing of the bottom atom layers kept the cell in place and an infinite lattice was mimicked by keeping the cell borders at the desired temperatures at all times. More details of previous similar simulations are found in [3].

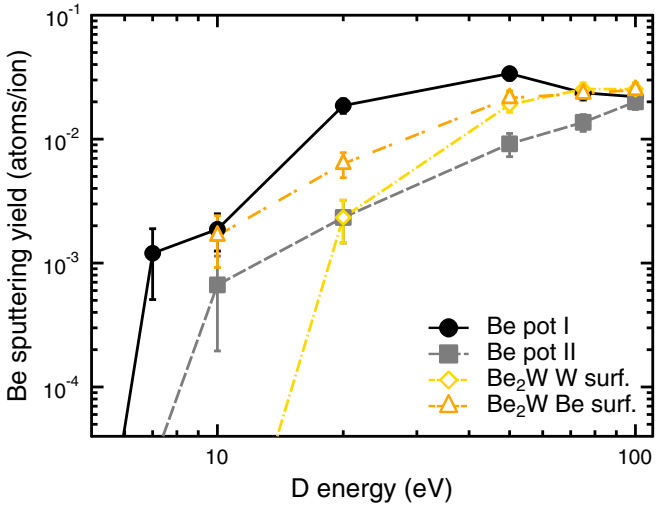

Figure 2. Simulated Be sputtering yield for different potentials and surfaces. The yield includes Be sputtered as single atoms and as part of a molecule.

3.2. Interatomic potentials

The classical interatomic potentials that were used are many-body bond-order potentials fitted to *ab initio* calculations and experimental values of both bulk and molecular properties. In the initially pure Be surface simulations, two versions of the Be–Be and Be–H potentials were used [31], here denoted *pot I* and *pot II*. The second parametrization is a variation of pot I and was developed in order to obtain good BeC alloy properties. There are only small differences between these potentials, e.g. in the cohesive energy (pot II −3.62 eV, pot I −3.32 eV), in the elastic constants and in the thermal expansion. Moreover, pot I has a slightly larger cut-off (pot I cut = 2.908 Å, pot II cut = 2.685 Å) and a non-zero μ value (related to an asymmetry term affecting the potential for atoms with different bond lengths). A possibly important quantity is also the surface binding energy, which was determined by giving a surface atom a specific kinetic energy directed normal to the surface. The surface binding energy was defined as the maximum energy at which the atom remained attached to the surface. At 300 K, this energy was ∼7.8 eV for pot I and ∼10.8 eV for pot II.

The Be–W potential from [30] was used, which is compatible with the pot II version of the Be–Be and Be–H interactions.

3.3. Results of the simulated sputtering

Figure 2 shows the total Be sputtering yield (i.e. including atomic Be and BeD molecules) obtained in the simulations at 300 K, both for Be and Be_2W surfaces. The yields are averaged over the whole bombardment sequence, i.e. over 3000 cumulative ion impacts. In pure Be, the yield is larger for pot I than for pot II, which is likely related to the higher surface binding of pot II. The yields do not depend on temperature, as they were seen to be similar at 300, 450 and 725 K (using pot II). The Be yield in the Be_2W case depends on the initial top layer as the W surface layers in the beginning act protectively,

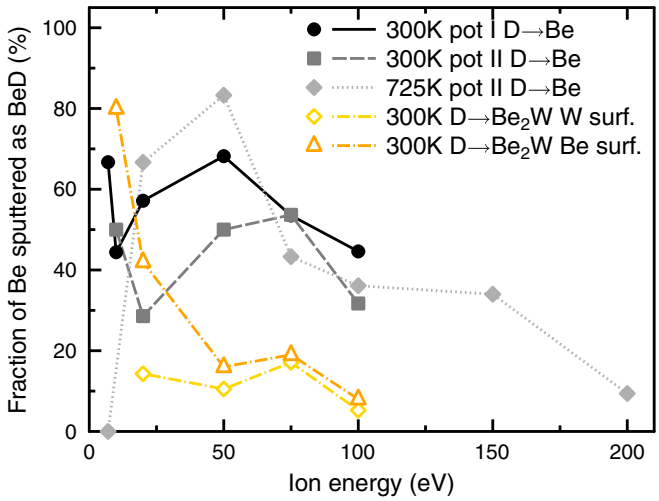

Figure 3. Fraction of BeD molecules of the total amount of sputtered Be from pure Be and Be_2W surfaces. Data for different potentials and temperatures are shown.

resulting in a low Be sputtering and high threshold. At higher energies, the difference is not visible as the D ions can here cause relatively more mixing of the top layers, bringing Be from sub-surface layers up to the surface. No W was sputtered in any of the simulations.

Release of BeD molecules was also observed in the simulations. Figure 3 plots the fraction of these, defined as the number of BeD molecules divided by the total number of released Be, as a function of incoming D energy. The fraction is seen to decrease with increasing energy as observed in PISCES-B measurements as well [33]. (Note that the 10 eV data point of the 725 K pot II simulations is represented by only one sputtering event; the release of a BeD_2 molecule. Similarly, the 10 eV 300 K pot II point consists of one released BeD out of a total of two sputtering events.) This behavior indicates that the physical sputtering yield is more efficient than SCS as the energies become larger. The BeD fraction for Be_2W W-terminated surfaces is constantly low.

The statistical error is large at low energies as a lot of time consuming simulations are required to observe one single sputtering event since the yields are low. For instance, in the pot I 10 eV case, only nine sputtering events took place and four of these were the release of a BeD molecule.

For an illustration of the SCS mechanism, snapshots of a sputtering event during a 10 eV D ion impact resulting in the release of a D_2 and BeD molecule are shown in figure 4. The D ion is seen to penetrate in between two surface Be atoms, breaking their bond and thereafter attaching to a neighboring D atom. The weakly bonded Be surface atom receives enough momentum in the process to be able to move away from the surface together with one of its (initially four) D neighbors.

The angular distribution of the sputtered single Be and BeD molecules is plotted in figure 5. Both species are very close to a cosine distribution around the normal to the surface. The points include data from both pot I and pot II and all energies since the statistics for only one case were poor due to small sputtering yields. Figure 6 shows the same kind of distribution, but for the energy of the sputtered species. It is seen that both single Be atoms and the molecules are sputtered with a mean energy a lot higher than what is associated with thermal release, confirming that also the BeD molecules are released through a kinetic process, i.e. the SCS mechanism. The mean energy is somewhat lower for the BeD molecules. A slight dependence on the incoming ion energy was observed, with the mean peak at higher energies with increasing ion energy. Since most of the single atoms are sputtered at the higher ion energies, their energy distribution is thus shifted to higher energies. The opposite applies to the BeD molecules.

This different peak positions are also probably related to the surface binding. For illustration, a Thompson distribution $f(E) \propto (E/(E+U_b)^3)$, where U_b is the surface binding energy is added to figure 6 [35]. The distribution using two different values for U_b, 2 and 6 eV, is plotted. The energy distribution for the BeD molecules agrees better with the 2 eV case and the single Be atoms with the 6 eV case, indicating that the BeD molecules have a lower binding energy to the surface. The difference in the binding energy is explained as follows. At incoming ion energies of 10–20 eV, the D surface concentration is higher than for higher energies where the penetration depth is larger, which makes it more likely for any Be atom to have many D neighbors. The average number of D neighbors to any sputtered Be was calculated to be around 3 for 10 eV ion impacts and almost none at 100 eV [33]. This D bonding lowers the binding energy of the Be atom to the surface, making it more easily sputtered, which is also reflected in the sputtering energy.

4. Observation and simulations of BeD in a plasma

The MD simulations showed that BeD molecules can, in theory, be released from Be surfaces and that this happens through the SCS mechanism. Observations in the linear plasma simulator PISCES-B and in JET have shown that BeD sputtering also happens in real plasma surroundings [15, 16]. The observations in [15] support the hypothesis that the SCS mechanism is responsible for the release as the energy of the sputtered BeD was similar to that of the single Be sputtered atoms (~2 eV), excluding the possibility of a thermal release. Also, a similar decrease in the BeD fraction with ion energy as in the simulations was observed [33].

To take the comparisons between the experimental observations and the MD simulations further, we implemented the information gained from the MD simulations into the 3D Monte-Carlo plasma impurity code ERO [36] and applied the code to a plasma exposure measurement performed in PISCES-B. This step is required due to the different time and space scales of the methods: MD only covers a nano-scale part of the surface for a few picoseconds, whereas ERO can simulate the whole PISCES-B device including the surface and plasma volume for several seconds. Direct comparison with observed light emission is also possible with ERO. These advantages are unavoidably balanced by the lack of accuracy in the PWI modeling, something which the MD data here aim to improve.

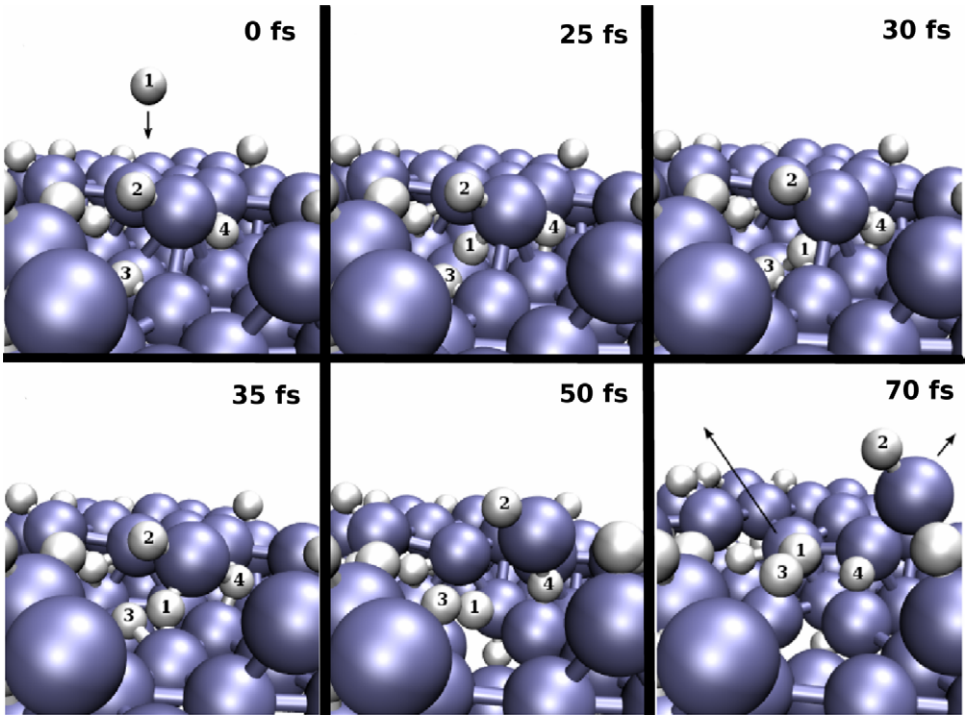

Figure 4. Illustration of the SCS mechanism. A 10 eV D ion (gray spheres) is impacting on a Be (violet spheres) surface, causing a D_2 and BeD molecule to be sputtered.

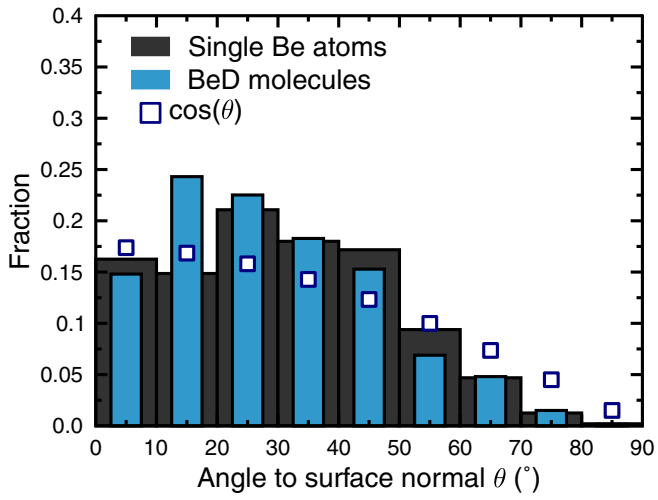

Figure 5. Simulated sputtering angle distribution of BeD molecules and Be atoms from a Be surface.

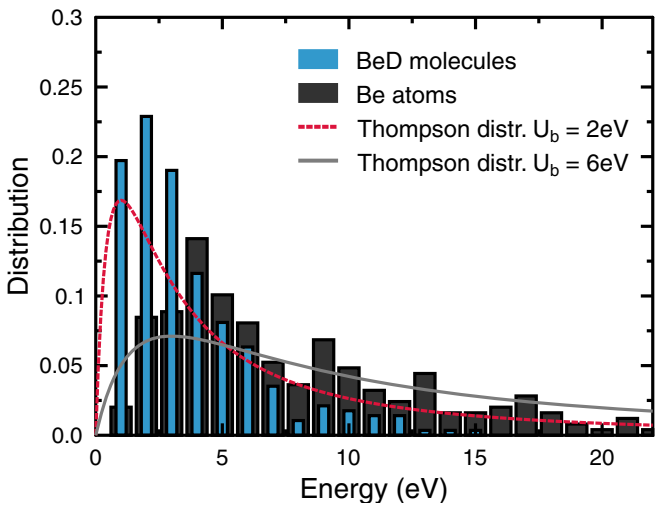

Figure 6. Energy distribution of sputtered Be and BeD. The incoming ion energies are in the range 7–200 eV. A Thompson distribution $f(E) \propto E/(E+U_b)^3$ with two different surface binding energies U_b is added for comparison.

4.1. PISCES-B experimental setup

Dedicated experiments were performed in PISCES-B in order to quantify the BeD release near a Be target. A polycrystalline Be target (S65C from Brush Wellman) was exposed to a D plasma and the BeD band emission ($A\,^2\Pi \rightarrow X\,^2\Sigma^+$, 497.3–499.2 nm) as well as several neutral and ionized atomic Be lines were spectroscopically measured along the plasma axis. The electron density and temperature measured at the plasma column axis at $z = 150$ mm from the target were $n_e = 2.6 \times 10^{18}\,\mathrm{m}^{-3}$ and $T_e = 8$ eV, respectively. The applied target bias range was -80 to -140 V, the plasma space potential -12 V, the pressure of neutral D_2 was 1.7 mTorr and the ion flux $3.2 \times 10^{22}\,\mathrm{m}^{-2}\,\mathrm{s}^{-1}$. The composition of molecular species in the plasma was calculated to be $(D^+, D_2^+, D_3^+) = (0.46, 0.46, 0.08)$ and the axial magnetic field was 0.0152 T.

4.2. ERO simulations

ERO is able to simulate erosion of a target due to plasma contact and the subsequent motion of the released species in the plasma. Possible re-deposition and -erosion can also be taken into account. The code uses the test-particle approximation and considers friction, thermal forces, cross-field diffusion,

ionization, dissociation and neutral collisions. A more detailed description of the code is found in, e.g., [36, 37].

To simulate the particular case of PISCES-B plasma geometry, n_e was assigned a Gaussian radial profile and an axial one corresponding to the measured D_γ line. The ion temperature was set to $T_i = 1/5T_e$ and was like the electron temperature constant axially as well as over the whole target. Elastic collisions with neutral D_2 molecules were included.

Important for the ERO simulations are the PWI processes, namely both the single Be and BeD sputtering yields due to not only background D plasma but also due to returning Be and BeD ions. Due to the vast uncertainty range in the experimentally measured Be sputtering yields, no clear choice for these parameters exist. Here we use the above MD simulation results for D impact and the yields from [31] were applied for both Be and to the few returning BeD molecules.

The sputtering yields determine the number of atoms released from the Be surface, but the behavior of the sputtered particles in the plasma is largely determined by the rate at which reactions (ionization, excitation and dissociation) take place due to electron (and proton) collisions in the plasma. The ADAS database [38] was used to describe the electron collision rates for Be reactions in the plasma. The cross-section (σ) for the BeD reactions, including non-dissociative ionization, dissociative excitation (via a series of pre-dissociating BeD excited states), as well as the excitation cross-section ($X\,^2\Sigma^+$; $v_i = 0 \rightarrow A\,^2\Pi$; $v_f = 0$) transition were calculated as described in [39]. The dissociative recombination cross-section of BeD^+ was taken from [40]. The final rate coefficients $\langle\sigma v\rangle(T_e)$ were calculated by integrating the cross-sections with a Maxwellian electron energy distribution. The rates are dependent on the vibrational state of the molecule, and here it was assumed that BeD is released from the surface in its first excited vibrational level, $v = 1$, as observed [12].

We also simulated the BeD sticking probability with MD needed for the ERO simulations. Both rotating and non-rotating molecules were allowed to impact on a pure Be surface or a surface containing around 30% D. It was seen that the molecules stick with a higher probability to a surface with added D. At an impact energy of 0.1 eV, the sticking probability was around 9% and at 100 eV only 0.5%. These numbers were used for describing the sticking of neutral BeD and BeD ions in ERO, respectively.

4.3. Comparison of simulated and observed sputtering yields

The absolute Be and BeD sputtering yields were not determined in the present experiment. Comparisons with earlier measurements [41] using a similar target and simulations using the pot I potential, however, showed that the MD yields were larger than the PISCES-B yields by a factor of around 20 (see figure 7 and [39]). The pot II yields are smaller than the pot I yields, meaning that they are closer to the experimental ones. Figure 7 shows the experimental yields together with the MD values that are corrected with the molecular content of the plasma for that particular experiment $(D^+, D_2^+, D_3^+) = (0.25, 0.47, 0.28)$, assuming that the D_2^+ and D_3^+ impact the surface as two D atoms with one half and three

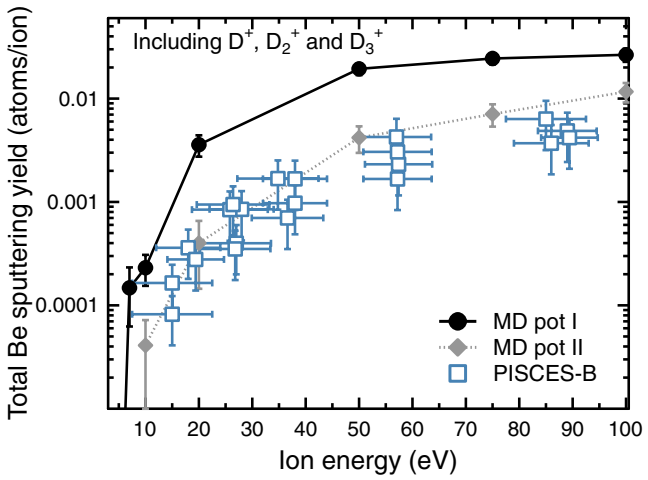

Figure 7. The total Be sputtering yield according to MD using two different potentials and PISCES-B measurements. The MD yields are corrected assuming $(D^+, D_2^+, D_3^+) = (0.123, 0.463, 0.414)$ in the plasma (see text). The PISCES-B data are from [39].

D atoms with one third of the energy of D^+, respectively. The corrected yield, here defined as sputtered Be per incoming ion (in the form D^+, D_2^+ or D_3^+), was calculated according to

$$Y = f_{D^+} \times Y_{D^+}(E_{D^+}) + f_{D_2^+} \times Y_{D^+}\left(\frac{E_{D^+}}{2}\right) + f_{D_2^+} \times Y_{D_2^+}\left(\frac{E_{D^+}}{3}\right),$$

where f denotes the molecular fractions weighed by the amount of D in respective molecule. In the above case

$$f_{D^+} = \frac{0.25}{0.25 \times 1 + 0.47 \times 2 + 0.28 \times 3} = 0.123,$$

$$f_{D_2^+} = \frac{0.47 \times 2}{0.25 \times 1 + 0.47 \times 2 + 0.28 \times 3} = 0.463 \quad \text{and}$$

$$f_{D_3^+} = \frac{0.28 \times 3}{0.25 \times 1 + 0.47 \times 2 + 0.28 \times 3} = 0.414.$$

Y_{D^+} is the yield calculated from the impact of only D ions with an energy E_{D^+}. This energy is defined as the ion charge times the difference between the applied bias voltage and the measured plasma space potential, $E = q(U_{bias} - U_{plasma})$. Both potentials are negative. Although pot II shows a better agreement with the observed values, one cannot definitely conclude that pot II is superior to pot I since these PISCES-B yields are only one of many measured yields, including ion beam experiments, that are scattered in a range of a few orders of magnitude (see, e.g., [33, 42, 43] for further discussion). Also, the sputtering yields are one of many properties of a material, meaning that an overall performance of a potential is very difficult to assess. The melting behavior of Be is, for instance, better described by pot I.

The BeD fraction of the total sputtering yield was calculated from the spectroscopic measurements, resulting in a constant fraction of ~17% at all applied biases, which is in contrast to the expected decreasing behavior with increasing bias (i.e. ion energy) seen by MD and earlier measurements. This is due to the fact that the sample temperature was not kept constant and the BeD yield has been observed to be dependent

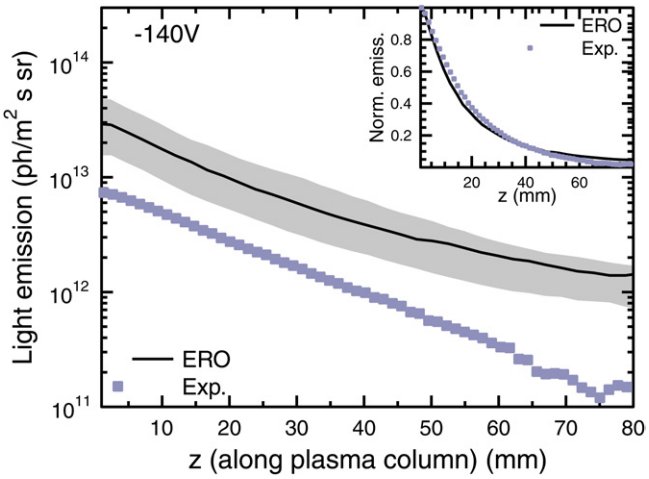

Figure 8. The light emission intensity profile of BeD at applied bias −140 V. Both experimental measurements and simulation results are shown. The gray area shows the range related to uncertainties in plasma parameters. The inset illustrates the normalized emission profiles. Sputtering yields according to case 2 are used.

on this temperature, with a maximum around 450 K which is believed to be related to the breakup of BeD_2 molecules [14] (BeD_2 molecules were not detected). Two versions of the sputtering yields were therefore used in the ERO simulations: case 1: Both single Be and BeD sputtering yields are according to pot I and case 2: The total yield is that of pot II, and 83% of that is single Be and 17% is BeD.

4.4. Modelled and observed BeD emission in the plasma

The light emission profiles of the sputtered BeD molecules when the applied bias was −140 V and the case 2 sputtering yields were used are plotted in figure 8. The inset includes the normalized profile and it illustrates excellent agreement between the experimental measurements and the simulations. The normalization is performed so that the maximum of the light emission for each bias is normalized to the maximum at −80 V. A factor of 4 difference is found when comparing the absolute values of the light emission (7 for bias −80 V). Using the sputtering yields according to case 1, on the other hand, the BeD light is overestimated in ERO by a factor of ∼30–70 depending on the bias, showing that the sputtering yield of case 2 is better suited for this experiment, as expected. Case 1 was also used in [39], where an even larger overestimation was found for slightly different plasma conditions (higher density, lower temperature and a higher neutral D_2 pressure).

Since both the light emission and number of sputtered species heavily depend on the plasma condition, we checked whether or not the uncertainties in the measured plasma parameters could explain the overestimation of ERO when using the case 2 sputtering yields. We therefore changed the electron density and temperature to account for the experimental error bars (estimated as 20% and 2 eV for the electron density and temperature, respectively). This resulted in the gray area in figure 8. The minimum of the gray area is now close to the experimental curve, with a difference that can be ascribed to the uncertainties in the spectroscopic database and/or in the sputtering yields.

The same order of magnitude values for the experimental and simulated atomic neutral Be 332 and 457 nm line emission intensities can also be obtained when taking the above error bars into account (factors ranging from 7–15 depending on the bias).

5. Conclusions

It was shown that the swift chemical sputtering mechanism could occur in both covalent materials and metals by simulating D bombardment of Be and Be_2W surfaces. SCS was seen to be responsible for BeD release from both surfaces. The sputtering yields of Be_2W alloys were dependent on the initial top surface layers and preferential sputtering of Be was observed. In pure Be, on the other hand, the interatomic potential affects the results and a crucial parameter of the potential is believed to be the surface binding energy. The total sputtering of the potential with a relatively higher binding energy was seen to agree better with measured PISCES-B yields.

ERO was applied to a dedicated PISCES-B experiment. When distributing the total sputtering yields obtained by MD into BeD and single Be sputtering branches according to experimentally estimated ratios (17% BeD), good agreement was found for the light emission intensities of the different species. The BeD emission profiles match perfectly, showing that the BeD transport is well described in ERO. The results also showed that in order to be able to quantitatively reproduce experimental spectroscopic observations, the sputtering yield of both single Be and BeD of that particular experiment needs to be known as the transport of these species after release is different and no universal yields of Be exist.

Acknowledgments

CB gratefully acknowledges grants from the Academy of Finland. This work was partly carried out under the US DOE Contract: DE-FG02-07ER54912. It was also supported by the European Communities under the contract of Association between EURATOM/FZJ, and was carried out within the framework of EFDA. The views and opinions expressed herein do not necessarily reflect those of the European Commission. CPU time for computations has been provided by JSC (Jülich Supercomputer Centre).

References

[1] Parker R, Janeschitz G, Pacher H D, Post D, Chiocchio S, Federici G and Ladd P, ITER Joint Central Team and Home Teams 1997 Plasma–wall interactions in ITER *J. Nucl. Mater.* **241–243** 1–26

[2] Roth J *et al* 2008 Tritium inventory in ITER plasma-facing materials and tritium removal procedures *Plasma Phys. Control. Fusion* **50** 103001

[3] Kirschner A, Wienhold P, Phillips V, Coad J P, Huber A, Samm U and JET EFDA contributors 2004 Modelling of carbon transport in fusion devices: evidence of enhanced re-erosion of *in-situ* re-deposited carbon *J. Nucl. Mater.* **328** 62

[4] Tokunaga K, Baldwin M J, Doerner R P, Nishijima D, Kurishita H, Fujiwara T, Araki K, Miyamoto Y, Ohno N and Ueda Y 2009 Nanoscale surface morphology of tungsten materials induced by Be-seeded D–He plasma exposure *J. Nucl. Mater.* **417** 528–32

[5] Doerner R P, Luckhart S C, Seraydarian R, Sze F C and Whyte D G 1999 Plasma interactions with mixed-material plasma facing components *Phys. Scr.* **T81** 35–39

[6] Doerner R P 2007 The implications of mixed-material plasma-facing surfaces in ITER *J. Nucl. Mater.* **363–365** 32–40

[7] Linsmeier Ch, Luthin J and Goldstrass P 2001 Mixed material formation and erosion *J. Nucl. Mater.* **290–293** 25–32

[8] Nishijima D, Baldwin M J, Doerner R P and Yu J H 2011 Sputtering properties of tungsten 'fuzzy' surfaces *J. Nucl. Mater.* **415** S96–9

[9] Hopf C, von Keudell A and Jacob W 2003 Chemical sputtering of hydrocarbon films *J. Appl. Phys.* **94** 2373

[10] Vietzke E, Refke A, Phillips V and Hennes M 1997 Energy distributions and yields of sputtered C_2 and C_3 clusters *J. Nucl. Mater.* **241–243** 810–5

[11] Oyarzabal E, Doerner R P, Shimada M and Tynan G R 2008 Carbon atom and cluster sputtering under low-energy noble gas plasma bombardment *J. Appl. Phys.* **104** 043305

[12] Stangeby P C, Auciello O and Haasz A A 1983 Chemical sputtering of carbon by sub-eV atomic hydrogen: new results and a critical comparison with previous data relevant to fusion applications *J. Vac. Sci. Technol.* A **1** 1425

[13] Krstic P S, Reinhold C O and Stuart S 2007 Chemical sputtering from amorphous carbon under bombardment by deuterium atoms and molecules *New J. Phys.* **9** 209

[14] Nishijima D, Doerner R P, Baldwin M J, De Temmerman G and Hollmann E M 2008 Properties of BeD molecules in edge plasma relevant conditions *Plasma Phys. Control. Fusion* **50** 125007

[15] Doerner R P, Baldwin M J, Buchenauer D, De Temmerman G and Nishijima D 2009 The role of beryllium deuteride in plasma–beryllium interactions *J. Nucl. Mater.* **390–391** 681–4

[16] Duxbury G, Stamp M F and Summers H P 1998 Observations and modelling of diatomic molecular spectra from JET *Plasma Phys. Control. Fusion* **40** 361

[17] Wiltner A and Linsmeier Ch 2006 Surface alloying of thin beryllium films on tungsten *New J. Phys.* **8** 181

[18] Linsmeier Ch, Ertla K, Roth J, Wiltnera A, Schmida K, Kosta F, Bhattacharyyaa S R, Baldwin M and Doerner R P 2007 Binary beryllium–tungsten mixed materials *J. Nucl. Mater.* **363–365** 1129–37

[19] Doerner R P, Baldwin M J and Causey R A 2005 Beryllium–tungsten mixed-material interactions *J. Nucl. Mater.* **342** 63

[20] Baluc N 2006 Materials for fusion power reactors *Plasma Phys. Control. Fusion* **48** B165–77

[21] Shimizu R 1986 Preferential sputtering *Nucl. Instrum. Methods Phys. Res.* B **18** 486–98

[22] Nishijima D, Baldwin M J, Doerner R P and Seraydarian R 2007 Parametric studies of carbon erosion mitigation dynamics in beryllium seeded deuterium plasmas *J. Nucl. Mater.* **363** 1261–5

[23] Eckstein W, Dohmen R, Mutzke A and Schneider R. SDTrimSP: A Monte-Carlo code for calculating collision phenomena in randomized targets, http://edoc.mpg.de/287291

[24] Karetta F and Urbassek H M 1992 The dimer sputtering mechanism of Cu(001) at low bombarding energy *Appl. Phys.* A **55** 364

[25] Vörtler K, Björkas C and Nordlund K 2011 The effect of plasma impurities on the sputtering of tungsten carbide *J. Phys.: Condens. Matter* **23** 085002

[26] Nordlund K, Björkas C, Vörtler K, Meinander A, Lasa A, Mehine M and Krasheninnikov A V 2011 Mechanism of swift chemical sputtering: comparison of Ce/C/W dimer bond breaking *Nucl. Instrum. Methods Phys. Rev.* B **269** 1257–61

[27] Salonen E, Nordlund K, Keinonen J and Wu C H 2001 Swift chemical sputtering of amorphous hydrogenated carbon *Phys. Rev.* B **63** 195415

[28] Krasheninnikov A V, Nordlund K, Salonen E, Keinone J and Wu C H 2002 Sputtering of amorphous hydrogenated carbon by hypothermal ions as studied by tight-binding molecular dynamics *Comput. Mater. Sci.* **25** 427–34

[29] Nordlund K 2006 PARCAS computer code. The main principles of the molecular dynamics algorithms are presented in
Nordlund K, Ghaly M, Averback R S, Caturla M, Diaz de la Rubia T and Tarus J 1998 Defect production in collision cascades in elemental semiconductors and FCC metals *Phys. Rev.* B **57** 7556–70
Ghaly M, Nordlund K and Averback R S 1999 Molecular dynamics investigations of surface damage produced by keV self-bombardment of solids *Phil. Mag.* A **79** 795
Nordlund K 1995 Molecular dynamics simulation of ion ranges in the 1–100 keV energy range *Comput. Mater. Sci.* **3** 448

[30] Björkas C, Henriksson K O E, Probst M and Nordlund K 2010 A Be–W interatomic potential *J. Phys.: Condens. Matter* **22** 352206

[31] Björkas C, Juslin N, Timko H, Vörtler K, Henriksson K, Nordlund K and Erhart P 2009 Interatomic potentials for the Be–C–H system *J. Phys.: Condens. Matter* **21** 445002

[32] Nordlund K, Salonen E, Krasheninnikov A V and Keinonen J 2006 Swift chemical sputtering of covalently bonded materials *Pure Appl. Chem.* **78** 1203–12

[33] Björkas C, Vörtler K, Nordlund K, Nishijima D and Doerner R 2009 Chemical sputtering of Be due to D bombardment *New J. Phys.* **11** 123017

[34] Okamoto H and Tanner L E 1991 *Phase Diagrams of Binary Tungsten Alloys* ed S V Nagendra Naidu and P Ramo Rao (Calcutta: Indian Institute of Metals)

[35] Goehlich A, Gillmann D and Döbele H F 2000 Angular resolved energy distributions of sputtered atoms at low bombarding energy *Nucl. Instrum. Methods Phys. Res.* B **164–165** 834–9

[36] Kirschner A, Philipps V, Winter J and Kögler U 2000 Simulation of the plasma–wall interaction in a tokamak with the Monte Carlo code ERO-TEXTOR *Nucl. Fusion* **40** 989

[37] Borodin D *et al* 2010 Modelling of impurity transport in the linear plasma devices PISCES-B and Pilot-PSI using the Monte-Carlo code ERO *Contrib. Plasma Phys.* **3–5** 432–8

[38] ADAS User Manual 2004 version 2.6. http://adas.phys.strath.ac.uk

[39] Björkas C *et al* 2012 Multiscale modelling of BeD release and transport in PISCES-B *Proc. J. Nucl. Mater., PSI-2012 Conf.* accepted

[40] Roos J B, Larsoon M and Larsson Å 2009 Dissociative recombination of BeH^+ *Phys. Rev.* A **80** 012501

[41] Nishijima D, Doerner R P, Baldwin M J and De Temmerman G 2009 Erosion yields of deposited beryllium layers *J. Nucl. Mater.* **390–391** 681

[42] Doerner R, Björkas C, Nishijmaa D and Schwarz-Sehnger T 2012 Spectroscopic measurements of Be erosion at JET ILW and interpretation with ERO modelling *Proc. J. Nucl. Mater., PSI-2012 Conf.* accepted

[43] Borodin D *et al* 2012 Measurements of gross and net erosion of beryllium *Proc. J. Nucl. Mater., PSI-2012 Conf.* accepted